doi:10.2533/chimia.2022.288 Chimia 76 (2022) 288–293

Enhancement of Power-to-Gas *via* Multi-catalyst Reactors Tailoring Reaction Rate and Heat Exchange

Emanuele Moioli*

SCS-Metrohm Award for best oral presentation in Catalysis Sciences & Engineering

Abstract: The Sabatier reaction is a key element of the power-to-gas development. For this reason, even though the process is known for more than a century, the Sabatier reaction is currently the object of important research efforts towards the development of new catalysts for performance improvement. However, the industrial exploitation of the Sabatier reaction depends on the development of reactors that match the best catalyst with an appropriate heat management. For this reason, this paper develops a methodology for the contemporary optimization of the reactor concept and the catalysts. It is observed that the reactor can be divided into three sections with contrasting requirements. In the first section, the main requirement concerns the reach of the reaction activation conditions. Hence, an adequate match between catalyst and reactor is needed, for example with an appropriate pre-heater. Once the reaction is activated, a reaction hotspot is formed, so that the cooling becomes determining and the main requirement for the catalyst is the resistance to poisoning and sintering. In the last section of the reactor, the low temperature activity of the catalyst is determining, so that a high-performance catalyst is needed. This paper indicates a strategy for the rational design of this catalyst, based on mechanistic evidence.

Keywords: Catalyst design · CO_2 methanation · Heat transfer · Reactor optimization

Emanuele Moioli received his PhD from the Friedrich-Alexander-Universität Erlangen-Nürnberg, Germany, in 2018, under the supervision of Prof. Hannsjörg Freund. During his PhD as Marie-Curie Fellow, he had several research stays as guest scientist at Lonza Specialty Ingredients, Visp, Switzerland. He then moved to the Ecole Polytechnique Fédérale de Lausanne for a postdoctoral stay in the group of Prof. Andreas Züttel, working on an Innosuisse project in collaboration with Gaznat. Since 2020, he is working as scientist at the Paul Scherrer Institute, where he is developing new reactors for power-to-X applications, connected with waste valorization and biomass utilization.

1. Introduction

The Sabatier reaction (also called CO_2 methanation) has gained significant interest over the last few years, thanks to the hypothesis that renewable H_2 will be widely available at low cost in the future.[1] The process to synthesize synthetic methane from renewable electricity is often referred to as power-to-gas. The reaction follows the stoichiometry:

$$CO_2 + 4H_2 \rightleftharpoons CH_4 + 2H_2O \qquad \Delta H_R^0 = -165.1\ kJ/mol \tag{1}$$

On the common catalysts used for the Sabatier reaction, also the reverse water gas shift (RWGS) reaction occurs:

$$CO_2 + H_2 \rightleftharpoons CO + H_2O \qquad \Delta H_R^0 = +41.2\ kJ/mol \tag{2}$$

At the same time, the produced CO can react with H_2 in the CO methanation reaction (linear combination of the two previous reactions):

$$CO + 3H_2 \rightleftharpoons CH_4 + H_2O \qquad \Delta H_R^0 = -206.3\ kJ/mol \tag{3}$$

The reaction takes place over several metal-based catalysts, including Ni,[2–4] Co[5–7] and Ru.[8–10] All the above-mentioned catalysts show high selectivity to methane, but only Ru is active at sufficiently low temperature to achieve almost complete CO_2 conversion. In fact, the Sabatier reaction is limited by thermodynamics, so that high conversion is possible only below 300 °C.[11] Additionally, the current regulations for product injection in the natural gas grid are stringent. For example, the maximum allowed H_2 content in the gas grid in Switzerland is 2 vol./vol.%.[12] This often requires the installation of post-treatment units (*e.g.* membranes) to achieve the required gas purity.[13] For all these reasons,

*Correspondence: Dr. E. Moioli, E-Mail: emanuele.moioli@psi.ch
Energy and Environment Division, Paul Scherrer Institute, Forschungsstrasse 111, CH-5232 Villigen

significant research activities focused on the development of new catalysts, which combine the low cost granted by non-noble metals (*e.g.* Ni) with high activity.[14] However, the management of the Sabatier reaction goes beyond the catalyst design, as the industrial scale reactors show important elements of non-ideality, such as the presence of temperature hotspots. These may cause the instauration of significant transport limitations.[15,16] Hence, the optimally performing Sabatier reactor should be the sum of several optimization aspects, combining reactor and catalyst design in an appropriate way.

In order to address these elements, this paper develops an appropriate methodology to match reaction kinetics and transport phenomena, with the goal of designing the most cost-effective Sabatier reactor. In this sense, several different considerations are needed. First, an appropriate kinetic model for a reference catalyst is required. For the Sabatier reaction, numerous kinetic models are available both for the Ni-based and for Ru-based catalyst. Several of these models were recently summarized by Hernandez Lalinde *et al*.[17] (Ni-based) and by Falbo *et al*.[18] (Ru-based). The kinetic model allows the determination of the optimal trajectory a fluid particle should follow in the reactor, in order to minimize the size and cost of the equipment. This optimization can be performed, for example, with the methodology developed by Peschel *et al*.[19] In this way it is possible to identify sections of the reactor that are characterized by different requirements, in terms of rate-determining mechanism. For the Sabatier reactor, it was determined that the course of the reaction is characterized by three separated zones with different heat transfer requirements.[20] Initially, it is necessary to deliver heat to the reactants, to assure the reaction activation.[21,22] Later, once the reaction is started, the reactor requires intense cooling, due to the exothermicity of the process.[23,24] At the end of the reactor, the temperature must be kept constant to match thermodynamics and kinetics.[20] The determination of these different sections of the reactors has an important influence on the catalyst design, as each is characterized by a different dominating reaction mechanism and a different selectivity to the various products. This paper shows how to adapt the properties of the catalyst (independently from the active material chosen) in agreement with the design choices to yield an optimal reactor in terms of both reaction engineering and catalysis.

2. Methodology

2.1 *Catalyst Synthesis*

0.5 wt./wt.% Ru/Al_2O_3 was purchased from Sigma Aldrich. The pristine Ni and Co powders were purchased from Goodfellow (London, England). The main properties of the materials can be found in previous publications.[6,25] The powders were examined for purity by means of X-ray photoelectron spectroscopy (XPS) and no impurities other than oxygen and carbon on the surface were detected. XRD powder analysis was conducted, confirming the XPS results, showing that there are no impurities in the pristine metal catalysts. The pristine materials are used as purchased. The $Ni/Mn/TiO_2$ catalyst is synthesized by wet impregnation. The titania support was an AEROXIDE TiO2 P-25 (Evonik), characterized by high specific surface area (BET surface area 50 m^2/g) and by the presence of both rutile and anatase crystal structures. $Ni(NO_3)_2{\cdot}6H_2O$(99.9%) and $Mn(CH_3COO)_2{\cdot}4H_2O$ (99.9%) from Sigma-Aldrich were used as Ni and Mn precursors without further purification. In the synthesis procedure, $Ni(NO_3)_2{\cdot}6H_2O$ (0.297 g) and $Mn(CH_3COO)_2{\cdot}4H_2O$(0–0.501 g) were dissolved in 6 mL deionized H_2O. An appropriate amount of TiO_2 (*ca.* 2 g) was slowly added to the aqueous solution under stirring at room temperature. The resulting suspension was heated to 80 °C after 3 h to remove excess H_2O. The obtained solid was finally dried overnight at 110 °C in a static air oven. The Co/CoO catalysts are synthesized *in situ* starting from Co_3O_4. This precursor is reduced in H_2 with various temperature/time profiles to produce several self-supported catalysts with controlled ratios of Co and CoO, $Co_x(CoO)_{1-x}$ ($0 < x < 1$). Co_3O_4 was obtained by calcination of $Co(NO_3)_2{\cdot}6H_2O$ (Sigma-Aldrich, 98%) at 300 °C for 12 h followed by a temperature ramp of 2 °C min^{-1} to 400 °C and then continued calcination for 2 h at 400 °C. To quantify the fraction of metallic cobalt on the surface of the $Co_x(CoO)_{1-x}$ catalysts, samples were transferred to the XPS through a glovebox to avoid surface oxidation by the air. The XPS was equipped with a dual anode X-ray source and a Phoibos 100 (SPECS GmbH) hemispherical energy analyzer. The Mg Kα (1253.6 eV) source was used for this study. The survey and narrow scans were collected at 90 eV and 20 eV pass energy, respectively.

2.2 *Experimental Setups*

The pristine metal experiments described in this paper were carried out in a gas controlling and analysis system equipped with three mass flow controllers (MFC). The reaction products were analysed and quantified by a mass spectrometer (MS-Pfeiffer OmniStar 320), using the calibration procedure and partial pressure determination described in ref. [26]. The MFCs are of the Bronkhorst El Flow series. The flow range is 0.4–20 ml/min and the absolute measurement error in ml/min is 0.1% of the maximum set point (20 ml/min) plus 0.5% of the set point. The reactor is a stainless-steel tube with a diameter of 7 mm in the reaction zone. The reaction zone starts 75 mm after the gas inlet. The catalyst is inserted after a small layer of glass wool is added on top of the in-tube sintered steel filter (Swagelok SS-2F-K4-60). The depth of the catalyst bed is measured to calculate the space velocity. The catalyst is then topped by another layer of glass wool in order to keep the material in place towards the reactor outlet.

The mechanistic investigations for the $Ni/Mn/TiO_2$ catalyst were performed by Quick X-ray Absorption Fine Structure (QEXAFS) and by SSITKA. The oxidation state and structure of the Ni and Mn phases were studied during catalyst reduction using QEXAFS. Measurements were done at the Ni K-edge (8.3 keV) and the Mn K-edge (6.5 keV) in transmission mode on beamline B18 at Diamond Light Source (Didcot, United Kingdom). In a typical SSITKA measurement, 200 mg catalyst was loaded into the stainless-steel reactor tube after dilution with SiC. The sample was reduced by heating in 50 mL/min of 20 vol % H_2 in Ar at a rate of 5 °C/min to 450 °C followed by an isothermal dwell of 2 h. The reactor was subsequently cooled in the same gas flow to 200 °C, and the total pressure was increased to 2 bar. Further details can be found elsewhere.[27,28]

The mechanistic investigations for the Ru/Al_2O_3 and for the Co/CoO_x catalysts were performed using a Bruker Tensor 27 spectrophotometer with a resolution of 2 cm^{-1}, equipped with the Praying Mantis accessory and high-temperature reaction chamber (HVC) from Harrick Scientific for the diffuse reflectance infrared Fourier transformation spectroscopy (DRIFTS). The chamber was connected to He (purity 99.999%), H_2 (purity 99.999%), and CO_2 (purity 99.998%) gas lines and a turbomolecular pump. The background pressure was 1×10^{-5} mbar. The spectrophotometer was continuously flushed with clean dry compressed air. The peak assignment was done with a autonomous bi-level evolutionary Gaussian fitting (BEGF) procedure.[29]

2.3 *Reactor Modelling*

The design of the Sabatier reactor is performed by solving the mass and heat balances in a 1D heterogenous reactor model (Eqns (4)–(7)):

$$\frac{d(uc_i)}{dz} = k_g a_v (ci_b - ci_s) \quad (4)$$

$$(u\rho_b c_{tot})\frac{dT}{dz} = h_f a_v (T_s - T) + \frac{4}{d_{tube}} U_T (T - T_e) \quad (5)$$

$$k_g a_v (ci_b - ci_s) = \nu_{i,wgs}\eta\rho_b r_{wgs} + \nu_{i,sab}\eta\rho_b r_{sab} \quad (6)$$

$$h_f a_v (T_s - T) = \eta\rho_b(-\Delta H_{wgs}) r_{wgs} + \eta\rho_b(-\Delta H_{sab}) r_{sab} \quad (7)$$

The cooling medium is a thermal oil with inlet temperature of 200 °C. The catalyst efficiency factor is calculated *via* the Thiele modulus:

$$\phi = \frac{V_p}{S_p}\sqrt{\frac{(n+1)}{2}\cdot\left(\frac{k c_{i,s}^{n-1}}{D}\right)} \quad (8)$$

$$\eta = \frac{3}{\phi^2}(\phi\coth(\phi) - 1) \quad (9)$$

The heat transfer is calculated as:

$$\frac{1}{U_A} = \frac{1}{k_i} + \frac{k_c}{ln\left(\frac{r_i}{r_e}\right)} + \frac{1}{k_e} \quad (10)$$

k is calculated considering a stagnant and a dynamic contribution:

$$k = k_0 + 0.024 \cdot \frac{l \cdot Re}{d_p} \quad (11)$$

The kinetic models used for the simulations are specified in the results and discussion section.

3. Results and Discussion

3.1 *Catalyst Isothermal Performance*

In order to fully understand the basic performance of Ni, Co and Fe in the Sabatier reaction, the reactivity of the pristine materials was tested by recording the CO_2 conversion in the range 200–550 °C. The results are shown in Fig. 1. As a benchmark, the reactivity of the commercial Ru/Al_2O_3 catalyst is reported. All the curves are characterized by two different zones. Initially, the reaction is limited by kinetics, with the conversion progressively increasing with temperature. When the conversion approaches the thermodynamic equilibrium curve, the measured conversion decreases with the temperature, due to the prevalence of the thermodynamic limitations. The temperature of approach of the thermodynamic equilibrium is determining for the maximum CO_2 conversion which can be achieved over a certain material, with a lower onset temperature corresponding to a higher conversion. The onset temperature can be determined as the temperature where 15–20% CO_2 conversion is reached. Therefore, it is observed that cobalt activates at 280 °C and shows a maximum conversion of 70%. The Co curve is similar to the Ru/Al_2O_3 curve, with a temperature shift of *ca.* 30–40 °C, resulting in a *ca.* 10% lower CO_2 conversion. Ni is significantly less active in the Sabatier reaction, with an onset temperature of 380 °C and a maximum CO_2 conversion of 55%. As the maximum conversion is achieved at 530 °C, a significant amount of CO is co-produced. Fe shows a low activity in the Sabatier reaction, as confirmed by the high activation temperature (540 °C), which leads to a predominance of the RWGS reaction.

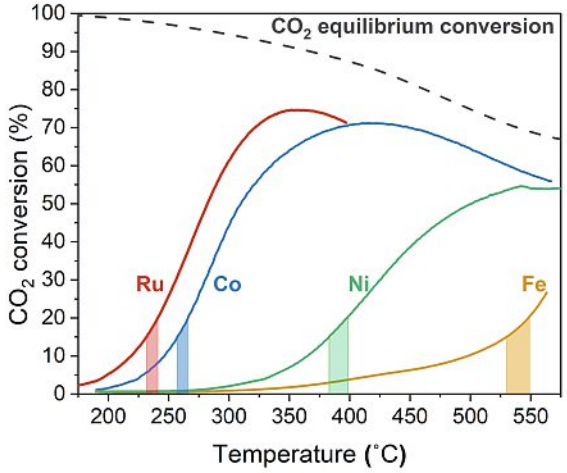

Fig. 1. The measured CO_2 conversion in the Sabatier reaction over Ru, Co, Ni and Fe. The shaded area refers to the temperature range for CO_2 conversion between 15 and 20%. (Conditions: P=1 bar, H_2:CO_2=4:1, SV=5000 h^{-1} for Ru/Al_2O_3 and SV=1000 h^{-1} for the other catalysts)

3.2 *Reactor Design*

The information on reactivity obtained so far in isothermal experiments should be supplemented by the knowledge of the concentration and temperature profiles to expect in an industrial-scale reactor operating with the same catalysts. The calculated methane yield vs. temperature profiles for Ru/Al_2O_3, Co and Ni are shown in Fig. 2. For Ru/Al_2O_3 and Ni the kinetic models by Falbo *et al.*[18] and by Xu and Froment[30] are used. These models are chosen because they describe well the experimental results of Fig. 1. For the Co-based catalyst, the kinetic model developed in ref. [25] was used.

The low-temperature activity of the catalyst determines the activation temperature of the reaction. For all the catalysts considered, the reactor is subject to parametric sensitivity. This means that a critical set of conditions exists, for which the heat production is sufficient to cause a sudden reactor runaway and the for-

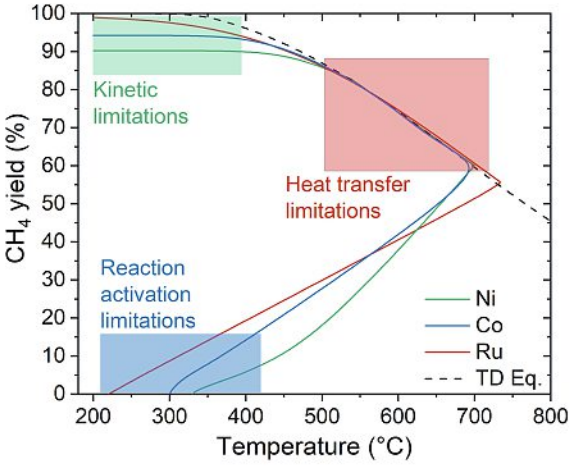

Fig. 2. The calculated methane yield vs. temperature for Ru, Co and Ni. It is possible to divide the reactor in three areas: a first section limited by reaction activation, a second zone with heat transfer limitations and a third section characterized by kinetic limitations. (Conditions: P=10 bar, H_2:CO_2=4:1)

mation of a significant temperature hotspot. This phenomenon in reference to the Sabatier reaction has been widely discussed in literature.[21,22] As the conditions of the simulated reactors are identical for the three catalysts, the different parametric sensitivity is reflected in a different reaction activation temperature. The reaction activation temperature is *ca.* 220 °C for Ru, 260 °C for Co and 340 °C for Ni. This corresponds approximately to the temperature for 10% CO_2 conversion in the isothermal tests reported in Fig. 1. As parametric sensitivity is a distinctive character for fixed-bed catalytic reactors operating the Sabatier reaction, it is hard to avoid the formation of a significant temperature hotspot.[31] This results in important challenges related to the handling of high temperature, but also gives the opportunity to utilize the high-temperature waste heat for process integration. In this sense, sufficient heat is available from the reaction to preheat the gas to the reaction activation temperature, even in the least favorable case of the Ni-based catalyst. Hence, in the design of the first section of the reactor, reaction engineering considerations are predominant over the catalyst design, as even a non-specific Ni-based catalyst can be successfully employed to initiate the reaction in an appropriately designed reactor.

Once the reaction is activated, the temperature rises until the gas mixture approaches the thermodynamic limit. In this section of the reactor, the reaction rates decrease drastically, due to the proximity to equilibrium. Hence, the heat transfer becomes limiting. In fact, the methane yield can increase only if the temperature is reduced. As the temperature is high, all the studied catalysts provide a sufficiently high reaction rate, so that the cooling rate is determining. This is visible in Fig. 2, where all the lines are overlap (light red area). However, special attention should be posed in this section to the possible problems related to catalyst deactivation. In fact, the high temperature may foster sintering phenomena as well as the possible catalyst poisoning due to CO formation in the RWGS reaction. For these reasons, an appropriate reactor design is essential to guarantee a good utilization of the catalyst and to minimize the equipment size. Efficient cooling can be achieved by maximizing the heat exchange surface and/or by enhancing the heat transfer (*e.g.* by using a boiling coolant).[20] The catalyst choice is less critical than the reactor design in this section, so that a cheap, transition metal-based catalyst can be used. In order to avoid deactivation phenomena, the use of a resistant catalyst, for example tested for methane steam reforming, may be recommended.[30,32,33]

When cooling lowers the temperature below *ca.* 400 °C, the reaction kinetics become determining. This is due to the reduced heat production, linked to the low amount of CO_2 and H_2 remaining. Hence, in this section, the catalyst gains a fundamental role in achieving the target methane yield. The dimensions of the reactor are here determined by the catalyst activity and by the possibility of reaching the required yield. If a catalyst is not suitable to achieve the desired yield, further purification steps in the downstream processing are needed.[34] For this reason, it is of general interest to synthesize appropriate catalysts that ensure the required productivity. Fig. 2 shows the final performance of the catalyst studied. Ru/Al_2O_3 is suitable to produce grid-compliant synthetic methane, because it is active at low temperature (*i.e.* below 220 °C). However, Ru is significantly expensive that an alternative catalyst would be highly desirable. Ni can reach a maximum CH_4 yield of *ca.* 90%, so that a significant performance improvement is needed. Co can reach 95% CH_4 yield, hence needing a limited optimization to reach the target result. Note that, in any case, the fraction of the reactor requiring a high-performing catalyst is limited.

3.3 *Catalyst Design*

In order to rationally design an effective catalyst, the mechanistic understanding of the reasons that make Ru highly active is necessary. To this end, a detailed *operando* analysis of the reaction intermediates in the Sabatier reaction over 0.5 wt./wt.-% Ru/Al_2O_3 catalyst was performed by means of DRIFTS.[35] It was observed that carbon monoxide (CO^*) adsorbed on the metallic surface is the key intermediate for methane production. This species is formed by decomposition of the adsorbed bicarbonate (HCO_3^{-*}), which in turn directly originates from the adsorption of CO_2 from the gas phase. Bicarbonate is formed at low temperature on the metal-support interface. Hence, the specific configuration of this specific adsorption site is essential for the low temperature activity of the catalyst. The reaction mechanism is schematized in Fig. 3: CO_2 is adsorbed on the support in various forms, according to the process conditions. The first key intermediate, HCO_3^{-*}, is formed at the metal-support interface. This species decomposes, in the presence of H_2, to produce the second key intermediate, CO^*, on the metallic surface. The optimal low-temperature performing catalyst should then provide the right combination of the different sites to maximize the reaction rate for these steps.

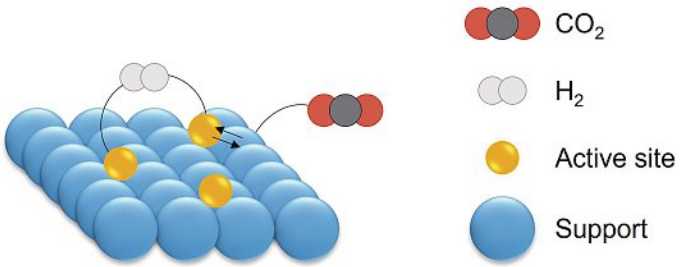

Fig. 3. The predicted general reaction mechanism: the active sites operate as H_2 adsorption location, while the support is the main adsorption site for CO_2, operating as carbon sink. The rate-determining step occurs at the interface between metal and support.

On the basis of this information, initially Co was targeted as active phase for the optimized catalyst. In order to produce sufficient interfaces between the metal and the support (CoO) the catalyst was synthesized *in situ* by reduction of Co_3O_4. The influence of the metallic Co fraction on the 20% CO_2 conversion temperature is shown in Fig. 4. The plot shows a clear minimum at 20% metallic Co fraction. This means that the low temperature activity of the Co-based catalyst can be significantly increased by tailoring the relative amount of metallic and oxidized sites. The analysis of the surface species by DRIFTS revealed that the enhanced activity of the sample with 20% metallic Co is due to a higher activity in the CO_2 adsorption and in the formation of oxygenated adsorbed species at the metal/support interface.[7] Hence, the control of the availability of the interface and the presence of an oxide support phase operating

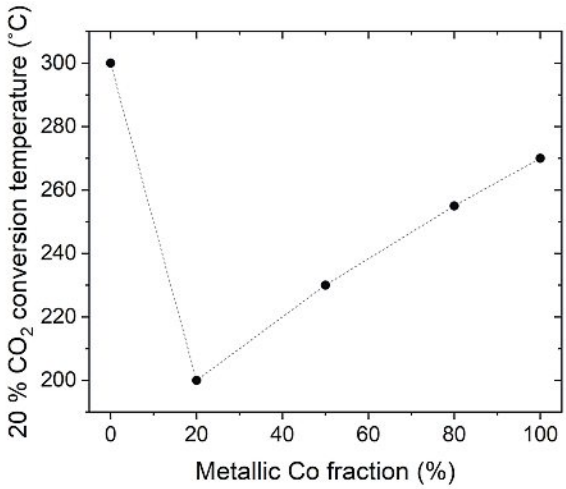

Fig. 4. The temperature required to achieve 20% CO_2 conversion at different metallic Co fractions in the Co/CoO catalysts (Conditions: P=1 bar, H_2:CO_2=4:1, SV=5000 h^{-1})

as reservoir for the adsorbed species is the key for the synthesis of a low-temperature active catalyst for the CO_2 methanation.

The same considerations formed the basis for the design of an optimized Ni-based catalyst. The enhancement of the Ni activity should follow the synthesis of an appropriate metal/support interface allowing the formation of the key intermediates of the CO_2 methanation. Since the pristine Ni shows scarce activity below 350 °C, it could be beneficial to improve the activity of the catalyst by addition of an appropriate promoter. First principle calculations showed that that Mn may be an appropriate promoter, as it decreases the energy barrier of CO_2 adsorption.[28] Hence a series of catalysts with different Mn:Ni ratios were synthesized by wet impregnation. Fig. 5 shows the temperature required to achieve 20% CO_2 conversion over these catalysts. The promoting effect of Mn is evident, as this reduces the onset temperature of *ca.* 60 °C. The optimal catalyst is composed of an equimolar

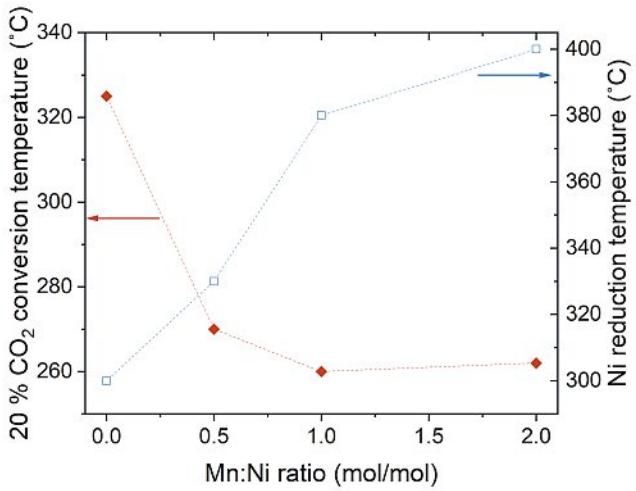

Fig. 5. The temperature required to achieve 20% CO_2 conversion and the temperature of Ni reduction (as measured by Ni K-edge XANES) at various Mn:Ni ratios (Conditions: P=1 bar, H_2:CO_2=4:1, SV=6000 h^{-1})

ratio of Ni and Mn. The mechanistic explanation of this enhanced performance lies in the reduced reduction temperature of Ni for the samples with significant Mn content. This was determined by TPH_2 with Ni K-edge XANES, as shown in Fig. 5. The Mn causes the formation of a optimal mixture of Ni^0 and Ni^{2+} hence providing the ideal amount of metal/support interface in the relevant conditions for CO_2 methanation.

3.4 *Optimal Reactor*

Fig. 6 shows the optimal reactor resulting from the previous considerations matching reaction engineering and catalyst design. The reactor is divided in three sections. In the first section, a simple Ni catalyst can be used, provided that the reaction activation is ensured by a careful preheating. This is done, for example, by recovering the heat from the product stream prior to water condensation or by using the waste heat from the reaction.

In the second zone, the heat transfer must be maximized, and the catalyst should be resistant to the high temperature of the reactor hotspot. This can be achieved, for example, by using a Ni/Mg/Al_2O_3 catalyst (from methane steam reforming) and a series of pipes with small diameter. In the last section, a tailored-made catalyst for the Sabatier reaction is required, to achieve high conversion. In this part of the reactor the only requirement for the reactor design is the preparation of isothermal conditions. The catalyst should instead be carefully designed to enhance the rate-determining step of the reaction, allowing the operation at low temperature. This last section can be operated both on Co or Ni, according to the specific requirements of the system to design. Note that the design of the previous sections is essential for the good functioning of this part of the reactor, because the eventual CO formed in the reaction hotspot should be converted prior to the inlet of this last zone. In fact, only by eliminating all the residual CO, is it possible to avoid deactivation phenomena due to blocking of the active sites on the metal/support interface.[28]

4. Conclusions

This paper showed how the interplay of reactor and catalyst design is essential to design an optimal process for the CO_2 methanation. Primarily, reaction engineering considerations are required to define the determining element among kinetics, thermodynamics, heat and mass transfer in the various section in which the reactor can be divided. These reflections already provide the indication of the optimal catalyst to employ, which, for some sections, may not correspond to the optimal catalyst for the target reaction. In fact, under certain conditions, side reactions may become dominating, hence the presence of additional components must be considered. When the reaction kinetics are not determining, the main focus should involve the design of an appropriate reactor configuration to minimize the effect of the other limiting factors. When, however, the reaction kinetics are determining, the optimal reactor directly depends on the maximization of the catalyst performance. It was shown that the rational design of an optimal catalyst should follow the determination of the essential characteristics that enhance the reaction rate. For the Sabatier reaction, the crucial element to establish is the correct ratio of oxidized and reduced sites, to ensure the formation of the CO_2 adsorption species and their fast conversion towards methane. It was shown that this is possible either by synthesizing *in situ* a catalyst with an appropriate formulation (in the Co case) or by adding a suitable promoter, adjusting the metal oxidation temperature (in the Ni case). The result of this unified reactor and catalyst design is an optimized reactor that combines all the required elements to maximize the productivity.

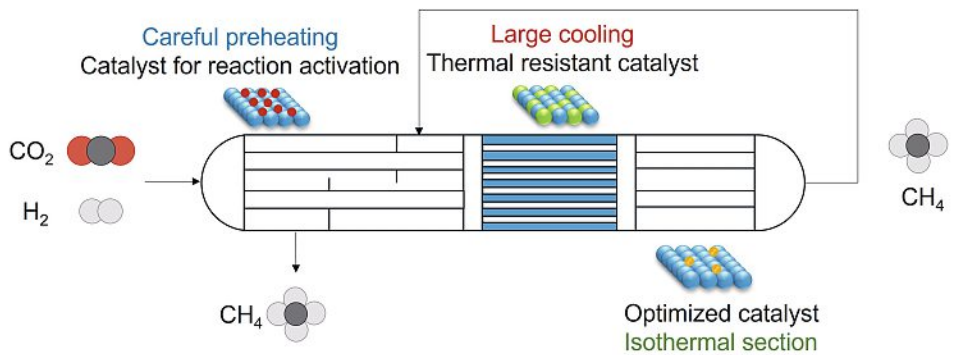

Fig. 6. The proposed reactor configuration, matching catalyst and reactor design.

This methodology, here applied to the Sabatier reaction, may be, in principle, extended to any catalytic reaction.

Acknowledgements

The author is grateful to the Swiss Chemical Society and Metrohm for the best oral presentation award. The author acknowledges funding of this work from the Innosuisse project 'Development of a Novel, Highly Efficient Energy System for Natural Gas Metering and Regulating Stations Based on Waste Heat Recovery and Synthetic Methane Production' (26441.1 PFIW-IW) and from the project 'Efficient Small-Scale Methanol Synthesis from Biogas' of the Swiss Federal Office of energy (project no. SI/502147). Part of this work was performed in the frameworks of the Energy Storage Integration (ESI) Platform of the Paul Scherrer Institute and of the Synfuels Initiative of the ETH board. The author gratefully acknowledges the contribution of Dr. Robin Mutschler, Dr. Kun Zhao, Prof. Andreas Züttel, Dr. Wilbert Vrijburg and Prof. Emiel Hensen in the preparation of the experimental results presented in the paper.

Received: January 21, 2022

[1] J. Gorre, F. Ortloff, C. van Leeuwen, *Appl. Energy* **2019**, *253*, 113594, https://doi.org/10.1016/j.apenergy.2019.113594.
[2] J. Kopyscinski, T. J. Schildhauer, F. Vogel, S. M. A. Biollaz, A. Wokaun, *J. Catal*. **2010**, *271*, 262, https://doi.org/10.1016/j.jcat.2010.02.008.
[3] F. Koschany, D. Schlereth, O. Hinrichsen, *Appl. Catal. B, Environ*. **2016**, *181*, 504, https://doi.org/10.1016/j.apcatb.2015.07.026.
[4] G. Garbarino, P. Riani, L. Magistri, G. Busca, *Int. J. Hydrogen Energy* **2014**, *39*, 11557, https://doi.org/10.1016/j.ijhydene.2014.05.111.
[5] G. D. Weatherbee, C. H. Bartholomew, *J. Catal.* **1982**, *77*, 460, https://doi.org/10.1016/0021-9517(82)90186-5.
[6] R. Mutschler, E. Moioli, W. Luo, N. Gallandat, A. Züttel, *J. Catal.* **2018**, *366*, 139, https://doi.org/10.1016/j.jcat.2018.08.002.
[7] K. Zhao, M. Calizzi, E. Moioli, M. Li, A. Borsay, *J. Energy Chem*. **2021**, *53*, 241, https://doi.org/10.1016/j.jechem.2020.05.025.
[8] P. J. Lunde, F. L. Kester, *Ind. Eng. Chem. Process Des. Dev*. **1974**, *13*, 27, https://doi.org/10.1021/i260049a005.
[9] A. Porta, L. Falbo, C. Giorgio, L. Lietti, C. Bassano, P. Deiana, *Catal. Today* **2019**, *343*, 38, https://doi.org/10.1016/j.cattod.2019.01.042.
[10] E. Moioli, R. Mutschler, A. Borsay, M. Calizzi, A. Züttel, *Chem. Eng. Sci. X* **2020**, *8*, 100078, https://doi.org/10.1016/j.cesx.2020.100078.
[11] J. Gao, Y. Wang, Y. Ping, D. Hu, G. Xu, F. Gu, F. Su, *RSC Adv*. **2012**, *2*, 2358, https://doi.org/10.1039/C2RA00632D.
[12] Schweizerischer Verein des Gas- und Wasserfaches SVGW/SSIGE, **2013**.
[13] J. Witte, J. Settino, S. M. A. Biollaz, T. J. Schildhauer, *Energy Convers. Manag*. **2018**, *171*, 750, https://doi.org/10.1016/j.enconman.2018.05.056.
[14] J. Gao, Q. Liu, F. Gu, B. Liu, Z. Zhong, F. Su, *RSC Adv*. **2015**, *5*, 22759, https://doi.org/10.1039/c4ra16114a.
[15] K. L. Fischer, M. R. Langer, H. Freund, *Ind. Eng. Chem. Res*. **2019**, *58*, 19406, https://doi.org/10.1021/acs.iecr.9b02863.
[16] J. Bremer, K. Rätzer, K. Sundmacher, *Aiche J.* **2017**, *63*, 23, https://doi.org/10.1002/aic.
[17] J. A. Hernandez Lalinde, P. Roongruangsree, J. Ilsemann, M. Bäumer, J. Kopyscinski, *Chem. Eng. J.* **2020**, *390*, 124629, https://doi.org/10.1016/j.cej.2020.124629.
[18] L. Falbo, M. Martinelli, C. G. Visconti, L. Lietti, C. Bassano, P. Deiana, *Appl. Catal. B Environ*. **2018**, *225*, 354, https://doi.org/10.1016/j.apcatb.2017.11.066.
[19] A. Peschel, H. Freund, K. Sundmacher, *Ind. Eng. Chem. Res*. **2010**, *49*, 10535, https://doi.org/10.1021/ie100476q.
[20] E. Moioli, N. Gallandat, A. Züttel, *Chem. Eng. J.* **2019**, *375*, 121954, https://doi.org/10.1016/j.cej.2019.121954.
[21] D. Schlereth, O. Hinrichsen, *Chem. Eng. Res. Des*. **2014**, *92*, 702, https://doi.org/10.1016/j.cherd.2013.11.014.
[22] E. Moioli, N. Gallandat, A. Züttel, *React. Chem. Eng*. **2019**, *4*, 100, https://doi.org/10.1039/C8RE00133B.
[23] A. El Sibai, L. K. Rihko Struckmann, K. Sundmacher, *Energy Technol.* **2017**, *5*, 911, https://doi.org/10.1002/ente.201600600.
[24] E. Moioli, A. Züttel, *Sustain. Energy Fuels* **2020**, *4*, 1396, https://doi.org/10.1039/c9se00787c.
[25] R. Mutschler, E. Moioli, A. Züttel, *J. Catal*. **2019**, *375*, 193, https://doi.org/10.1016/j.jcat.2019.05.023.
[26] R. Mutschler, W. Luo, E. Moioli, A. Züttel, *Rev. Sci. Instrum*. **2018**, *89*, https://doi.org/10.1063/1.5047402.
[27] W. Chen, R. Pestman, B. Zijlstra, I. A. W. Filot, E. J. M. Hensen, *ACS Catal*. **2017**, *7*, 8050, https://doi.org/10.1021/acscatal.7b02757.
[28] W. L. Vrijburg, E. Moioli, W. Chen, M. Zhang, B. Terlingen, B. Zijlstra, I. A. W. Filot, A. Zuttel, E. A. Pidko, E. J. M. Hensen, *ACS Catal*. **2019**, *9*, 7823, https://doi.org/10.1021/acscatal.9b01968.
[29] K. Zhao, L. Wang, E. Moioli, M. Calizzi, A. Züttel, *J. Phys. Chem. C* **2019**, *123*, 8785, https://doi.org/10.1021/acs.jpcc.8b11105.
[30] J. Xu, G. F. Froment, *AIChE J.* **1989**, *35*, 88, https://doi.org/10.1002/aic.690350109.
[31] R. Mutschler, E. Moioli, K. Zhao, L. Lombardo, E. Oveisi, A. Porta, L. Falbo, C. G. Visconti, L. Lietti, A. Züttel, *ACS Catal*. **2020**, *10*, 1721, https://doi.org/10.1021/acscatal.9b04475.
[32] T. T. M. Nguyen, L. Wissing, M. S. Skjøth-Rasmussen, *Catal. Today* **2013**, *215*, 233, https://doi.org/10.1016/j.cattod.2013.03.035.
[33] B. Mutz, H. W. P. Carvalho, S. Mangold, W. Kleist, J. D. Grunwaldt, *J. Catal*. **2015**, *327*, 48, https://doi.org/10.1016/j.jcat.2015.04.006.
[34] A. Gantenbein, J. Witte, S. M. A. Biollaz, O. Kröcher, J. Schildhauer, *Chem. Eng. Sci*. **2020**, 116012, https://doi.org/10.1016/j.ces.2020.116012.
[35] K. Zhao, L. Wang, M. Calizzi, E. Moioli, A. Zuttel, *J. Phys. Chem. C* **2018**, *122*, 20888, https://doi.org/10.1021/acs.jpcc.8b06508.